Calculated Charge Resolutions for Fast Current and Resonant Transformers

A. Reiter

December 2018

Contents

1 Introduction **2**

2 Fast Current Transformer **3**
2.1 Detector & Acquisition Scheme . . . 3
2.2 Signal Integration . . . 4
2.2.1 Beam Current and Charge . . . 4
2.2.2 Minimum charge quanta: uncertainty of single sample . . . 4
2.2.3 Uncertainty of Integral . . . 5
2.3 Estimate of Measurement Uncertainty . . . 6
2.3.1 Uncertainty without baseline correction . . . 6
2.3.2 Signal attenuation: pBar Production . . . 6
2.3.3 Signal amplification: 20 - 60 dB range . . . 6
2.3.4 Further comments . . . 7

3 Resonant Transformer in Transfer Line **8**
3.1 Detector & Acquisition Scheme . . . 8
3.2 Detector Signal . . . 8
3.2.1 Charge calculation . . . 8
3.2.2 Minimum charge quantum . . . 9
3.3 Measurement Uncertainty . . . 9
3.3.1 Offset correction . . . 9
3.3.2 Single maximum, single sample . . . 9
3.3.3 Single maximum, mean amplitude . . . 10
3.3.4 Further comments . . . 10

4 Conclusions and Summary **11**

1 Introduction

The subject of this document is the achievable resolution of charge measurements. The target value for the new detector systems at FAIR is the 1 % level. Two different detectors will be available at FAIR for this purpose:

- RT: Resonant transformer for measurements of the total charge Q_{tot} of a passing bunch or bunch train
- FCT: Fast current transformer for measurements of the instantaneous beam current $I(t)$. The charge Q_{tot} is derived by signal integration.

The two systems are briefly compared in Table 1 and described in separate sections 2 and 3. Time-domain and frequency spectra are presented in Fig. 1 for a SIS18 beam (h=4) measured at the HTP beam line. The resolution in both systems is defined on the front-end level by amplifier noise and on the acquisition side by ADC noise. These noise sources are regarded as independent. On the basis of available hardware parameters, mainly the effective number of ADC bits (ENOB), charge resolutions for a short pulse are calculated. The results are compared in the last section.

Once prototype data acquisition systems for both detectors are available, an experimental verification can be carried out with a precision charge generator (currently under development) that all FAIR transformers will used for in-situ calibrations or alternatively a high-fidelity pulse generator together with a series resistor.

Table 1: Comparison of FCT and RT measurement systems

Variable	Fast Current Transformer	Resonant Transformer
Det. response	beam current	damped oscillation
V(t)	V(t)$\propto$ current I(t)	V(t)$\propto$ amplitude A(t;ω_0,λ)
Signal	fast, unipolar	slow, bipolar
Frequency range	broad band	narrow band
	$\nu \sim$[1–100] MHz	$\nu \sim$[10–100] kHz
Frequency spectrum	variable, pulse shape dep.	fixed, indep. of pulse shape
Charge Q	$Q_{tot} = \int I(t)dt$	$Q_{tot} = A_{max}$
Uncertainty σ_Q	depends on pulse shape	indep. of pulse shape
Baseline correction	typ. required	no droop
Calibration	result depends on shape	test pulse transformed
	(frequ. content) of test pulse	to standard RT response
Signal transport	frequ. dep. attenuation	quasi-DC, simple correction
Commercial product	yes, Co. Bergoz, France	no, GSI device

2 Fast Current Transformer

2.1 Detector & Acquisition Scheme

We consider a fast current transformer FCT in a high-energy beam transfer line that measures the instantaneous beam current $I(t)$ as function of time t, see Fig. 2. The sensitivity S_{FCT} is given in units of (V/A) with a typical value of $S_{FCT} = (0.5 - 10)$ V/A [1]. For FAIR a low sensitivity of S=0.5 V/A was chosen. Due to its high bandwidth of (200−700) MHz, depending on the chosen model, this detector is able to resolve the bunch structure of the heavy-ion beam.

The components of the data acquisition (DAQ) system are shown in Fig. 3:

- Attenuator & Amplifier Unit: The output signal is conditioned in a remote-controlled attenuator/amplifier unit (gain G) to adjust the signal level to the full scale range V_{FS} of the ADC. For calculations, we assume a perfect attenuator (no added noise) or refer to the amplifier model Femto DUPVA-1-60 [2] with 1.2 GHz bandwidth (BW) and five gain ranges of [20,.., 60] dB. Its RMS noise was estimated from a batch of 15 units for each gain with a 200 MHz digital oscilloscope:

Gain [dB]	20	30	40	50	60
$\sigma_V[mV_{RMS}]$@ 200 MHz (measured)	0.15	0.2	0.7	2.5	8.0
$\sigma_V[mV_{RMS}]$@ 1.2 GHz (scaled)	0.37	0.49	1.72	6.1	19.6
$\sigma_V[mV_{RMS}]$@ 1.2 GHz (data sheet)	0.17	0.5	1.7	5.3	17.0

  The scaler RMS values correspond well to the data sheet value of 500 pV/$\sqrt{Hz}$ (17 μV at full BW) of the manufacturer for gains above 20 dB. At the lowest gain setting the intrinsic ADC resolution of the oscilloscope (1 mV/div) contributes to the measurement. The data sheet value is used for estimates in the remainder of this document.

- Signal Transport: This step can cause insertion and transmission losses and we call the attenuation factor T. (High-quality coaxial cables or an optical link can be employed; the latter option at the expense of signal quality. For distances at the FAIR facility below 200 m, coaxial cables are the better choice.) It is assumed that this effect can be correct for, hence we set $T = 1$ for simplicity.

- Data Acquisition: A GSa/s ADC digitizes the signal. The ADC sensitivity S_{ADC} in units of (ch/V) is defined by the ratio of number of ADC channels, 2^N (N=nominal bit number), and full scale voltage V_{FS}. At FAIR, we will use the Struck 2.5 GSa/s ADC with 14 nominal bits and fixed ±1 Volt input range, hence, S_{ADC}=0.12 mV/ch [3]. The input referred noise of the AD9689 ADC chip is stated in the data sheet as 4.5 LSB(rms) and ENOB∼10 for a 155 MHz full scale signal (smallest listed frequency).

The ADC response in channel units, $ADC(t)[ch]$, to an instantaneous current $I(t)$ can be calculated from:

$$ADC(t)[ch] = I(t)[A] \cdot S_{FCT}[V/A] \cdot G \cdot T \cdot S_{ADC}[ch/V] + ADC_{off}(t)[ch] \quad (1)$$

The ADC offset, $ADC_{off}(t)$, is typically derived from a linear fit to the data set in a pre- and post-beam region outside the beam pulse, defined for example by two timing events "beam on" and "beam off" that are distributed by the general machine timing system to all DAQ systems.

2.2 Signal Integration

2.2.1 Beam Current and Charge

We rearrange equation 1 and calculate the beam charge from a number of N_S signal samples in the ADC data (acquired between times t_1 and t_2), where Δt is the sampling interval:

$$I(t)[A] = \frac{(\, ADC(t) - ADC_{off}(t)\,)[ch]}{S_{FCT}[V/A] \cdot G \cdot T \cdot S_{ADC}[ch/V]} \tag{2}$$

$$Q[As] = \int_{t_1}^{t_2} I(t)\, dt = \sum_{i=1}^{N_S} I(t_i)\Delta t \tag{3}$$

If the beam pulse signal has a length Δt_S, the theoretical number of signal samples N_S is given by $N_S = \Delta t_S/\Delta t = \Delta t_S \cdot R$, where $R = 1/\Delta t$ is the ADC sampling rate. In practical applications, the integral includes some baseline samples N_B around the current signal which do not contribute to the integral value, but to the measurement uncertainty.

2.2.2 Minimum charge quanta: uncertainty of single sample

Regarding amplifier and ADC as independent noise sources, we can distinguish three different minimum charge quanta. Let us consider an amplifier signal without noise at the ADC input. Then, the minimum nominal charge quantum ΔQ_{nom} for the ideal ADC is given by the product of minimum discernible nominal current ΔI_{nom} and sampling interval Δt:

$$\Delta Q_{nom} = \Delta I_{nom}\Delta t[As] = \frac{1[ch]\Delta t[s]}{S_{FCT}[V/A] \cdot G \cdot T \cdot S_{ADC}[ch/V]} \tag{4}$$

ADC noise spoils the nominal sensitivity and yields an effective current I_{eff} that can be resolved as the baseline is broadened, typically evaluated as RMS value σ_{ADC}. With ENOB=10 for the chosen ADC, $\sigma_{ADC} = 16$ ch. The minimum effective charge quantum ΔQ_{eff} is given by the product of effective current ΔI_{eff} and sampling interval Δt:

$$\Delta Q_{eff} = \Delta I_{eff}\Delta t[As] = \frac{\sigma_{ADC}[ch]\Delta t[s]}{S_{FCT}[V/A] \cdot G \cdot T \cdot S_{ADC}[ch/V]} \tag{5}$$

Further, amplifier noise σ_V reduces the available signal-to-noise ratio and adds to the total measurement uncertainty σ_{meas}. Using the independence of both noise sources, we calculate the measurement noise by adding both components in quadrature:

$$\sigma_{meas} = \sqrt{\sigma_V^2 + \sigma_{ADC}^2} \tag{6}$$

Measurement noise is often dominated by amplifier noise σ_V, especially for higher gain settings. Finally, the charge measurement resolution for a single sample now becomes:

$$\Delta Q_{meas} = \Delta I_{meas}\Delta t[As] = \frac{\sigma_{meas}[ch]\Delta t[s]}{S_{FCT}[V/A] \cdot G \cdot T \cdot S_{ADC}[ch/V]} \tag{7}$$

2.2.3 Uncertainty of Integral

The integral over the beam current defines the measurement uncertainty since the charge is calculated by dividing out all technical parameters which are constants. Borrowing from ref. [7] (section 5.1) on calculations of beam positions and setting $\sigma_V = \sigma_{meas}$:
Uncertainty of ADC integral without offset correction:

$$\sigma(Int) = \sigma_{meas} \cdot \sqrt{N_S + N_B} = \sigma_{meas} \cdot \sqrt{N_{tot}} \quad \text{for } N_S \text{ signal and } N_B \text{ baseline samples} \tag{8}$$

Uncertainty of ADC integral after offset correction: If the baseline offset O is estimated as mean value $< O >$ from N_O samples outside the charge calculation region (which includes N_S signal and N_B baseline samples), the uncertainty σ_O is given as:

$$\sigma_{<O>} = \frac{\sigma_{meas}}{\sqrt{N_O}} \tag{9}$$

This value is subtracted from all samples, and this step introduces a common correlation (see [6], chapter 4). The uncertainty of the integral Int_{corr} over the offset-corrected data is then given by:

$$\sigma(Int_{corr}) = \sigma_{meas} \cdot \sqrt{N_S + \frac{N_S^2}{N_O}} \quad \text{for signal samples only } (N_B{=}0) \tag{10}$$

$$\sigma(Int_{corr}) = \sigma_{meas} \cdot \sqrt{(N_S + N_B) + \frac{(N_S + N_B)^2}{N_O}} \quad \text{for all samples } (N_B > 0) \tag{11}$$

The correlation introduces an additional term proportional to the total number of samples N_{tot}^2. Hence, it is important to exclude baseline samples N_B from the integral calculation and to include a maximum number of baseline samples N_O in the calculation of the offset value O. Two examples may be instructive:

- If we assume $N_O \in [N_S,\, 2 \cdot N_S]$ and $N_B = 0$, the uncertainty increases by (22–40)%.
- However, if we assume $N_B = 2 \cdot N_S$ – which for short pulses or extraction at h=2 from SIS18 is not unlikely unless a sophisticated time-of-flight analysis is carried out to select a tight window around the pulse signal – the uncertainty is increased by a factor of $\sqrt{12} \sim 3.5$ if $N_O = N_S$.

Therefore, the FCT measurement uncertainty depends on the global pulse structure (shape and number of extracted pulses) which can increase the best case uncertainty (no offset correction and $N_B = 0$) by a factor up to 4. This observation should be remembered when we compare FCT and RT performance.

2.3 Estimate of Measurement Uncertainty

2.3.1 Uncertainty without baseline correction

Finally, we insert Eq. 8 into Eq. 2 and obtain for a short pulse without offset correction of the baseline the uncertainty of the measured charge:

$$\sigma(Q_{meas}) = \frac{\Delta t[s] \cdot \sigma(Int)[ch]}{S_{FCT}[V/A] \cdot G \cdot T \cdot S_{ADC}[ch/V]} \quad (12)$$

$$= \frac{\Delta t[s] \cdot \sigma_{meas}[ch] \cdot \sqrt{N_S + N_B}}{S_{FCT}[V/A] \cdot G \cdot T \cdot S_{ADC}[ch/V]} \quad (13)$$

2.3.2 Signal attenuation: pBar Production

For a triangular pulse of 50 ns length and 2.5x10^{13} protons (4 μC pulse charge), the 80 V maximum peak voltage must be attenuated by a factor 100 (G=0.01) in order to fit into the $\pm$1 V input ADC range. A 5 μC pulse charge would result in a 1 V full scale signal. Assuming favourable conditions $N_B = 0$, $T = 1$ and $\sigma_V = 0\,ch$ as the amplifier is replaced by an ideal attenuator:

$$\sigma(Q_{nom}) \sim 0.11\,\text{nC} = 110\,\text{pC} \quad (14)$$

Including ADC noise, we set $\sigma_{meas} = \sigma_{ADC} \sim 16$ ch using the ENOB data:

$$\sigma(Q_{meas}) \sim 1.76\,\text{nC} = 1760\,\text{pC} \quad (15)$$

For smaller attenuation values G the uncertainty improves accordingly and one obtains the following table for the case of signal attenuation:

Max. pulse charge 1 [e]	5 μC 3.1x10^{13}	500 nC 3.1x10^{12}	50 nC 3.1x10^{11}
Gain [dB]	-40	-20	0
$\sigma(Q_{meas})$ [pC]	1760	176	17.6
$\sigma(Q_{meas})$ [e]	1.1x10^{10}	1.1x10^{9}	1.1x10^{8}
$\sigma(Q_{meas})$ [% FS]	0.04	0.04	0.04

2.3.3 Signal amplification: 20 - 60 dB range

The measurement uncertainty for a triangular pulse of 50 ns length in case of amplification is based on amplifier and ADC noise. The following table presents for a set of pulse charges the correct gain setting, noise and measurement resolution. For gains above 40 dB the absolute charge resolution does not change significantly.

Max. pulse charge 1 [e]	5 nC 3.1x10^{10}	1.6 nC 1.0x10^{10}	0.5 nC 3.1x10^{9}	0.16 nC 1.0x10^{9}	50 pC 3.1x10^{8}
Gain [dB]	20	30	40	50	60
$\sigma_V[mV_{RMS}]$	0.17	0.5	1.7	5.3	17
σ_V[ch]	1.4	4.1	13.9	43.4	139.3
σ_{ADC}[ch]	16	16	16	16	16
σ_{meas}[ch]	16.0	16.5	21.2	46.3	140.2
$\sigma(Q_{meas})$ [pC]	1.75	0.57	0.23	0.16	0.15
$\sigma(Q_{meas})$ [e]	1.1x10^{7}	3.6x10^{6}	1.45x10^{6}	1.0x10^{6}	9.6x10^{5}
$\sigma(Q_{meas})$ [% FS]	0.04	0.04	0.04	0.1	0.31

2.3.4 Further comments

- The resolution may be improved by a factor of 2–3, if the bandwidth is reduced to 250-300 MHz as shown by the RMS measurements of the Femto amplifier.
- The uncertainty estimates are well below 1 % full scale. It is therefore likely that the achievable system resolution in the accelerator facility is dominated by external noise sources. For example the FCT signals at the HTP beam line show significant pickup of noise and distortions. The effectiveness of electromagnetic shielding will be of great importance in the hardware design.
- Attenuator and amplifier need to be carefully selected and must show a smooth frequency behaviour in order to avoid complex calibration or unfolding procedures.
- For the wideband 500–700 MHz FCT type in the synchrotrons, the position dependence of the FCT response introduces another, yet small source of uncertainty (<0.2 %/mm). The HEBT FCTs of type LLS (low-lateral sensitivity) have a smaller bandwidth of 230 MHz and a negligible offset dependence.

3 Resonant Transformer in Transfer Line

The treatment of the Resonant Transformer (RT) is based on reference [4].

3.1 Detector & Acquisition Scheme

The RT measures the total charge of a bunch or bunch train (also referred to as batch), if the integration time is much shorter than the oscillation period of the damped resonance excited by the passing charges.
Figure 4 shows the RT equivalent circuit and Fig. 5 a measured response. Resistance R, total inductance L_S and capacitance C determine the frequency of the damped resonance (typically between 10-30 kHz). The total inductance $L_S = n^2 \cdot L_0$ is calculated from the number of windings n and the inductance factor L_0, the inductance for a single turn. The bipolar voltage V_C generated across the capacitor is fed to a remote-controlled amplifier & calibration unit. At FAIR, the amplified signal is transported to the electronics room and digitised in a 100 MHz ADC with ±5 Volt input, 14 nominal bits and ENOB∼11 [5]. Hence, we have a nominal sensitivity S_{ADC}=0.6 mV/ch. The amplifier offers five measurement ranges of [10, 1] μC and [100, 10, 1] nC.

3.2 Detector Signal

To a pulse of length T the RT responds with a damped oscillation with decay time constant λ and angular frequency ω_0. Their respective values are given by the values of the LRC circuit components as follows:

$$\lambda[Hz] = \frac{R[\Omega]}{2 \cdot L_S[H]} \quad (1\ \mathrm{H} = 1\ \mathrm{Vs/A} = \Omega\ \mathrm{s}) \tag{16}$$

$$\omega_0[Hz] = \sqrt{\frac{1}{L_S[H] \cdot C[F]} - \lambda[Hz]^2} \tag{17}$$

$$V_C(t)[V] \approx \frac{-I_B[A] \cdot T[s]}{n\,C[F]} \cdot e^{-\lambda t}\, cos(\omega_0 t) \quad \text{for T<<1} \tag{18}$$

$$= \frac{-Q[As] \cdot c_{cal}}{n\,C[F]} \cdot e^{-\lambda t}\, cos(\omega_0 t) \tag{19}$$

In the last step we have introduced the dimensionless factor c_{cal} as an overall technical calibration constant of the RT amplifier electronics.

3.2.1 Charge calculation

In the most simple case, the total charge Q_{tot} can be derived from one maximum value of the oscillation defined by equation 19. After calibration, the full scale output voltage V_{FS} of +5 Volt corresponds to the charge maximum Q_{FS} of the set amplifier range:

$$Q_{tot}[As] = \frac{V_{max}[ch]}{V_{FS}[ch]} \cdot Q_{FS}[As] \tag{20}$$

3.2.2 Minimum charge quantum

The minimum nominal charge quantum ΔQ_{nom} is given by the minimum discernible nominal voltage step. For the 14 bit ADC, only 13 bits are available for the amplitude measurement of the bipolar signal:

$$\Delta Q_{nom} = \frac{1[ch]}{2^{14-1}} \cdot Q_{FS} \sim 1.2 \cdot 10^{-4} Q_{FS} \tag{21}$$

Again, the minimum effective charge quantum ΔQ_{eff} is given by ADC noise which spoils the theoretical resolution and yields the effective resolution σ_{ADC}=8 ch (ENOB∼11):

$$\Delta Q_{eff} = \frac{\sigma_{ADC}[ch]}{2^{14-1}} \cdot Q_{FS} \sim 9.8 \cdot 10^{-4} Q_{FS} \tag{22}$$

Taking into account amplifier noise, the charge measurement resolution for a single sample becomes

$$\Delta Q_{meas} = \frac{\sigma_{meas}[ch]}{2^{14-1}} \cdot Q_{FS} \tag{23}$$

where σ_{meas} is given by Eq. 6 as before.

3.3 Measurement Uncertainty

From a previous experiment with a new RT prototype amplifier at the high-energy beam line HTP (July 2018), the RMS noise of the ADC baseline is estimated to be σ_V ∼1.5 mV in ranges 1 μC, 100 nC and 10 nC, but the smallest range of 1 nC which showed a larger noise level of σ_V ∼3.0 mV. These data were acquired with a 16 bit Struck VME ADC.

3.3.1 Offset correction

Also the RT data must be corrected for offsets. Contrary to the case of the FCT, the offset does not depend on the sensor signal (no dynamic effects like droop due to AC coupling) and is - in principle - a fixed value. Therefore, the offset can be determined accurately from a set of baseline samples before/after the signal and is disregarded in the further treatment.

3.3.2 Single maximum, single sample

For a single sample of a maximum, the charge resolution for ranges above 1 nC is given by

$$\Delta Q_{meas} = \frac{\sigma_{meas}[ch]}{2^{13}[ch]} \cdot Q_{FS} \sim \frac{8.4[ch]}{2^{13}[ch]} \cdot Q_{FS} = 1.0 \cdot 10^{-3} Q_{FS} \tag{24}$$

For the 1 nC range, a factor of 2 must be applied.

Range	10 μC	1 μC	100 nC	10 nC	1 nC
$\sigma_V[mV_{RMS}]$	1.5	1.5	1.5	1.5	3.00
σ_V[ch]	2.5	2.5	2.5	2.5	3.0
σ_{ADC}[ch]	8	8	8	8	16
σ_{meas}[ch]	8.4	8.4	8.4	8.4	16.3
$\sigma(Q)$ [pC]	10250	1025	102.5	10.3	1.0
$\sigma(Q)$ [e]	$6.4{\cdot}10^{10}$	$6.4{\cdot}10^{9}$	$6.4{\cdot}10^{8}$	$6.4{\cdot}10^{7}$	$1.2{\cdot}10^{7}$

3.3.3 Single maximum, mean amplitude

After acquisition with an ADC of 10–100 MSa/s, more than a single ADC datum is available for the determination of the maximum voltage, e.g via the mean value. The number of samples can be estimated by the following argument:

- The requirement that the cosine function changes by less than 0.5%, leads to a range of acceptable angles [-5.7°, +5.7°] or roughly a 10° interval.
- Assuming an oscillation frequency of 30 kHz (upper limit), the acceptable time interval is about 1.0 μs long.
- For 100 MSa/s the number of available samples is 100, and the uncertainty of the mean value Q_{mean} is reduced by a factor of 10: $\sigma(Q_{mean}) \sim 0.1\sigma(Q_{meas})$

Range	10 μC	1 μC	100 nC	10 nC	1 nC
$\sigma(Q_{mean})$ [pC]	1024	102.4	10.2	1.0	0.2
$\sigma(Q)$ [e]	$6.4{\cdot}10^9$	$6.4{\cdot}10^8$	$6.4{\cdot}10^7$	$6.4{\cdot}10^6$	$1.2{\cdot}10^6$

Note that a parabolic fit to the maximum extends the useful analysis region. This approach can be implemented using analytic formulae to extract the maximum value.

3.3.4 Further comments

- The charge resolution will be improved if a larger fraction of the data is analysed, e.g. if more than one maximum or minimum is exploited. The decay time λ is well known and fixed as is the oscillation frequency ω_0. Therefore, an analytic fit to the data can be performed. Figure 5 shows a signal of roughly 5% FS which offers a large number of maxima or minima for analysis.
- Another option for charge calculation is the integral of the absolute signal $\int |V(t)|$ with offset correction (to eliminate the rectifying effect of noise by the $|\cdot|$ function), see for example Fig. 6. The calibration can be performed with the in-built precision charge pulser of the RT in the same manner as for the maximum voltage.

4 Conclusions and Summary

We summarise the best-case results for a single, 50 ns long, triangular pulse in Table 2 for both transformer types. For the FCT, no correction of the baseline offset has been assumed. For the stated pulse charge, the ADC voltage in the FCT DAQ system reaches 1 Volt full scale for the given gain setting. Remember that the FCT resolution is pulse-shape dependent and deteriorates for longer pulses, a pulse train or when offset correction is necessary, but may be improved by a factor of ∼3 by an upper frequency limit in the analysis. Uncertainties of the RT are given for the case of a single maximum. The resolution may be improved, if a larger number of extreme values is analysed. With the given assumptions, the RT resolution seems to be better by a factor of ∼1.5 compared to the FCT.

Table 2: Comparison of theoretical FCT and RT resolution estimates

Pulse charge	5 μC	500 nC	50 nC	5 nC	0.5 nC
FCT gain	0.01	0.1	1	10	100
[dB]	-40	-20	0	20	40
$\sigma(Q)$ [pC]	1760	176	17.6	1.75	0.23
$\sigma(Q)$ [e]	$1.1{\cdot}10^{10}$	$1.1{\cdot}10^{9}$	$1.1{\cdot}10^{8}$	$1.1{\cdot}10^{7}$	$1.45{\cdot}10^{6}$
RT range	10 μC	1 μC	100 nC	10 nC	1 nC
$\sigma(Q_{mean})$ [pC]	1024	102.4	10.2	1.0	0.2
$\sigma(Q)$ [e]	$6.4{\cdot}10^{9}$	$6.4{\cdot}10^{8}$	$6.4{\cdot}10^{7}$	$6.4{\cdot}10^{6}$	$1.2{\cdot}10^{6}$

Note that the sensitivity of both transformers can be increased by a factor of 10. For secondary beams FCTs with a sensitivity of S=5.0 V/A are available, while the RT sensitivity can be increased using a combination of smaller capacitor C and a smaller number of windings.

Finally, the achievable resolution depends on the noise level after installation. Spurious noise and systematic distortions have been observed at test installations in the high-energy beam line HTP, especially in the FCT signal. As the two transformers operate in different frequency domains these problems will originate most likely from different noise sources. The simple operational principle of the RT might be less prone to distortions. For operational flexibility (simultaneous transmission monitoring and pulse shape analysis) it seems advantageous to have two different charge measurement systems available in the same mechanical housing. As they are equipped with the same precision charge calibration pulser cross calibrations and long-term stability monitoring are greatly simplified.

References

[1] Fast Current Transformers by Bergoz Instrumentation, France; http://www.bergoz.com/

[2] Data sheet of 1 GHz broadband DUPVA-1-60 amplifier available at: https://www.femto.de/de/produkte/ghz-breitband-verstaerker/variable-verstaerkung-bis-1-2-ghz-dupva.html

[3] https://www.struck.de/sfmc01.html

[4] Michael A. Clarke-Gayther, "A High Stability Intensity Monitoring System for the ISIS Extracted Proton Beam", EPAC 96, Barcelona, 10-14th June 1996

[5] https://www.ohwr.org/projects/fmc-adc-100m14b4cha/wiki

[6] R. Barlow, "Statistics, A guide to the Use of Statistical Methods in the Physical Sciences", Manchester Physics Series, 2008

[7] A. Reiter, R. Singh, O. Chorniy, "Statistical Treatment of Beam Position Monitor Data", Beam Instrumentation Department GSI, GSI-LOBI-2015-04-TN, 2015

List of Figures

1 Comparison of FCT and RT signals. Top left: FCT current measured with an inverting Miteq amplifier in a 1000 ns acquisition window after fast extraction from SIS18 (h=4). Top right: Damped RT oscillation of 20 kHz observed over 3 ms. Bottom left/right: FFT spectra of FCT and RT signals, respectively, illustrate the different frequency domains of detector operation. 14

2 TOP: FCT raw signal (blue), acquired with inverting Miteq amplifier and attenuator unit. The baseline (green) was fitted in two regions before and after the signal. BOTTOM: Offset-corrected and scaled current signal in units of mA. 15

3 Schematics of FCT electronics. The FCT output signal is fed to an attenuator/amplifier unit. After transport to an electronics room the signal is acquired by an ADC in the DAQ system. For intermediate signal path length of ∼300–400 m coaxial cables can be used before signal attenuation favours transmission via optical fibres. 16

4 Schematics of RT (Fig. 1 of ref. [4]). The RT output voltage V_C is fed to an amplifier & calibration unit. After transport to an electronics room the signal is acquired in the DAQ system. 17

5 Raw data of RT response. 18

6 Absolute value or RT signal. Charge calculation may be based on the signal area, instead of the signal amplitude. 19

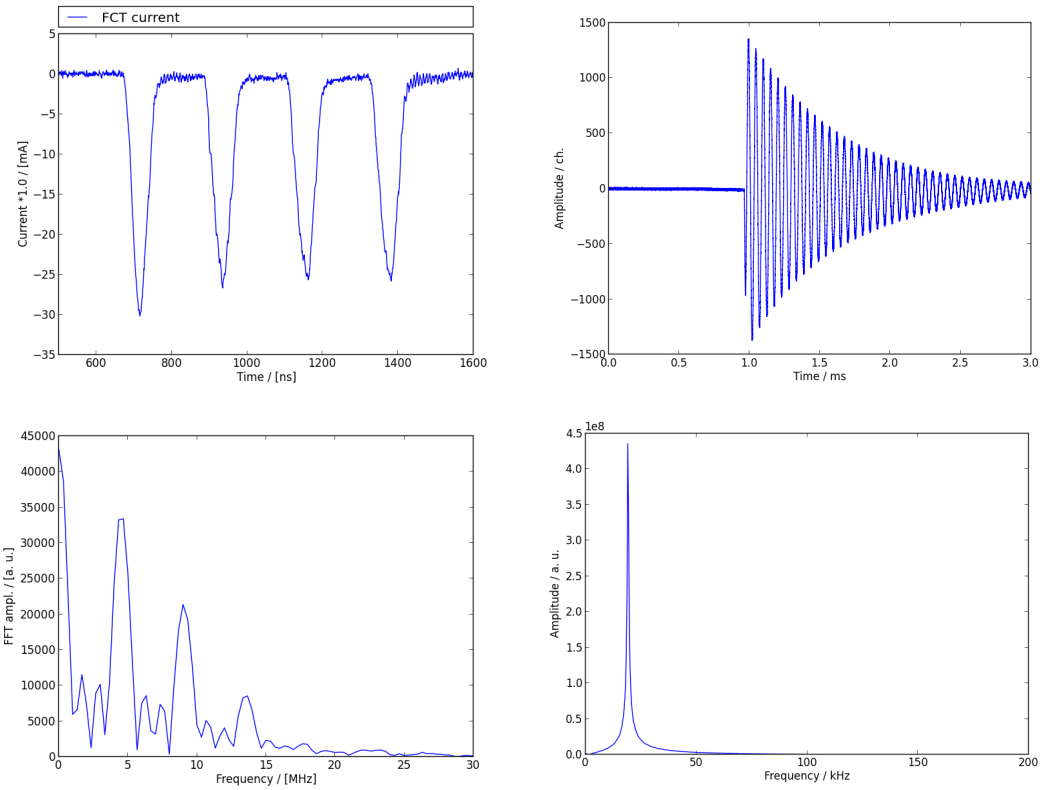

Figure 1: Comparison of FCT and RT signals. Top left: FCT current measured with an inverting Miteq amplifier in a 1000 ns acquisition window after fast extraction from SIS18 (h=4). Top right: Damped RT oscillation of 20 kHz observed over 3 ms. Bottom left/right: FFT spectra of FCT and RT signals, respectively, illustrate the different frequency domains of detector operation.

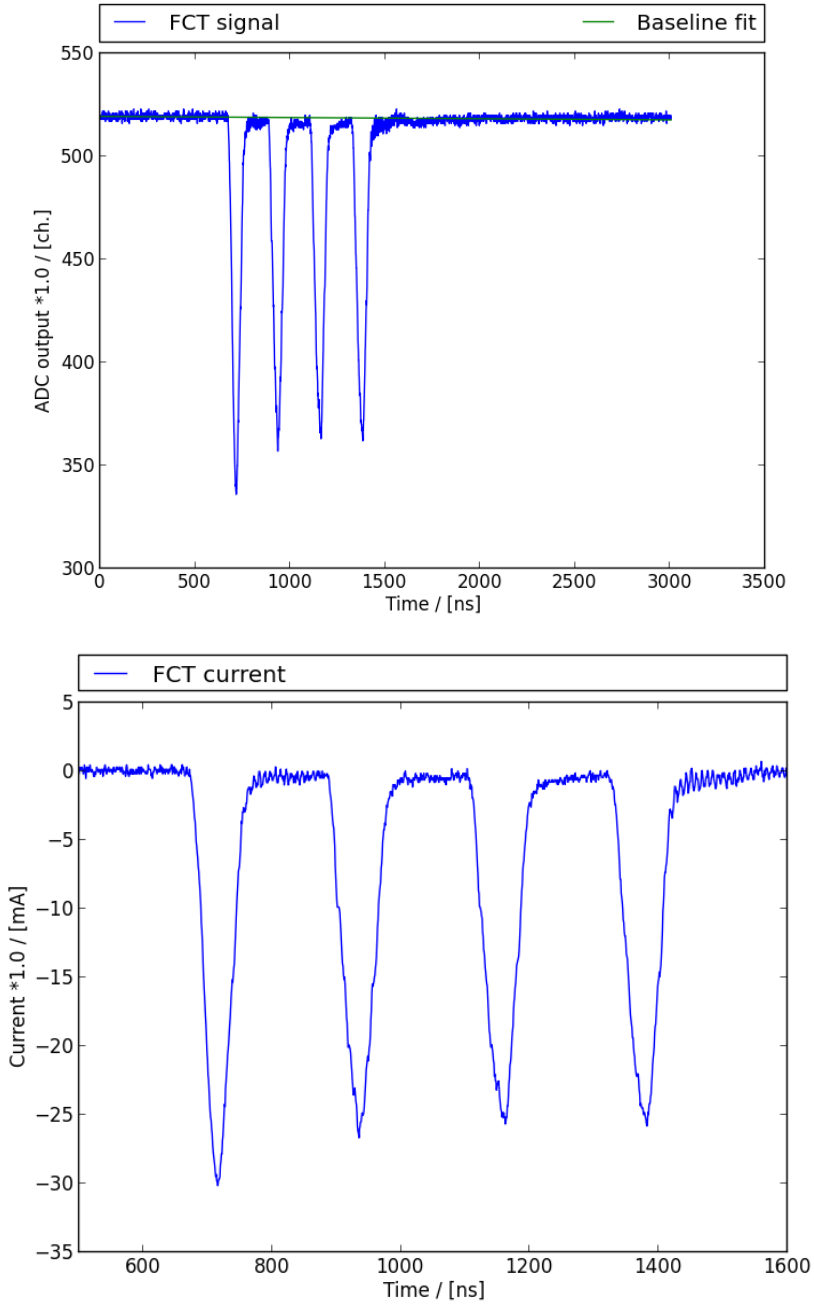

Figure 2: TOP: FCT raw signal (blue), acquired with inverting Miteq amplifier and attenuator unit. The baseline (green) was fitted in two regions before and after the signal. BOTTOM: Offset-corrected and scaled current signal in units of mA.

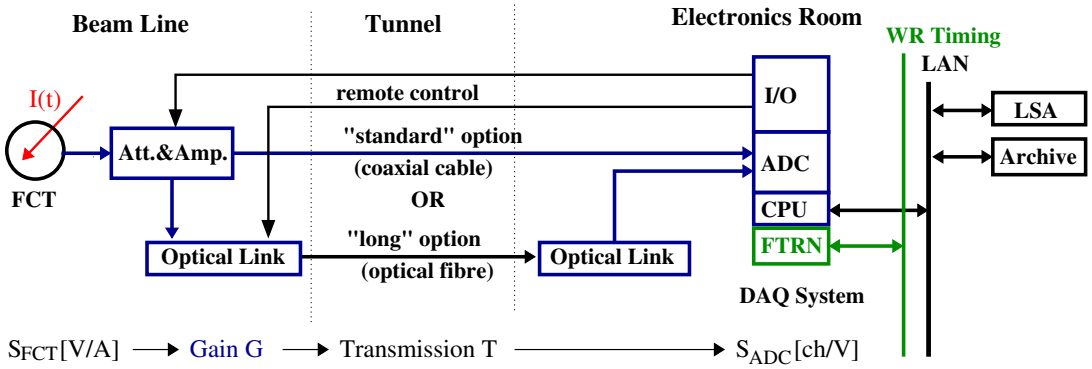

Figure 3: Schematics of FCT electronics. The FCT output signal is fed to an attenuator/amplifier unit. After transport to an electronics room the signal is acquired by an ADC in the DAQ system. For intermediate signal path length of ∼300–400 m coaxial cables can be used before signal attenuation favours transmission via optical fibres.

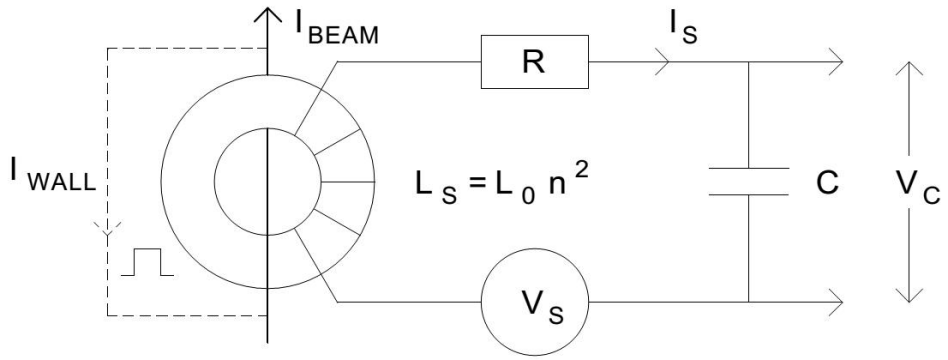

Figure 4: Schematics of RT (Fig. 1 of ref. [4]). The RT output voltage V_C is fed to an amplifier & calibration unit. After transport to an electronics room the signal is acquired in the DAQ system.

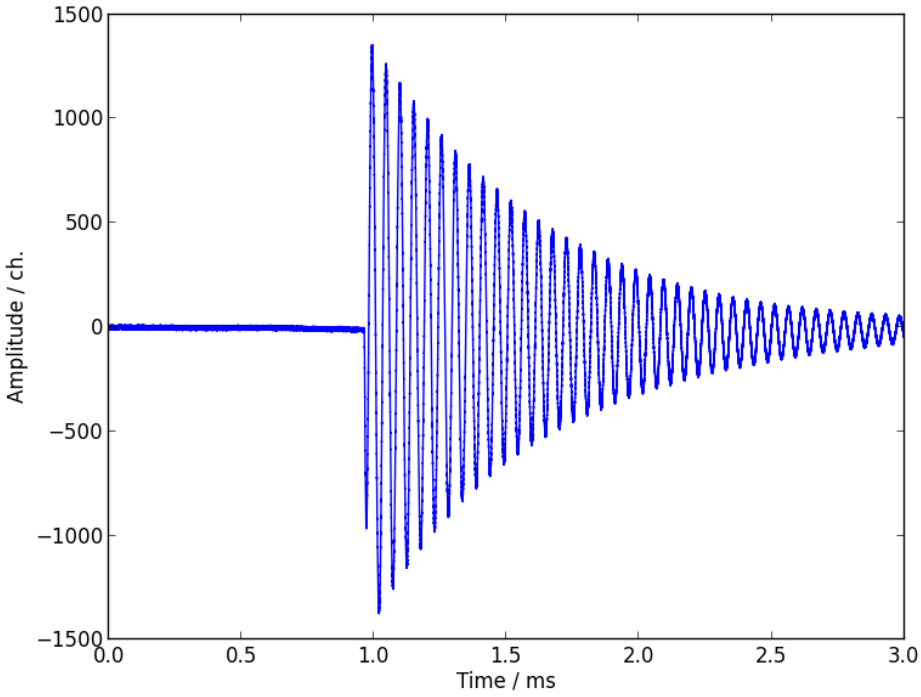

Figure 5: Raw data of RT response.

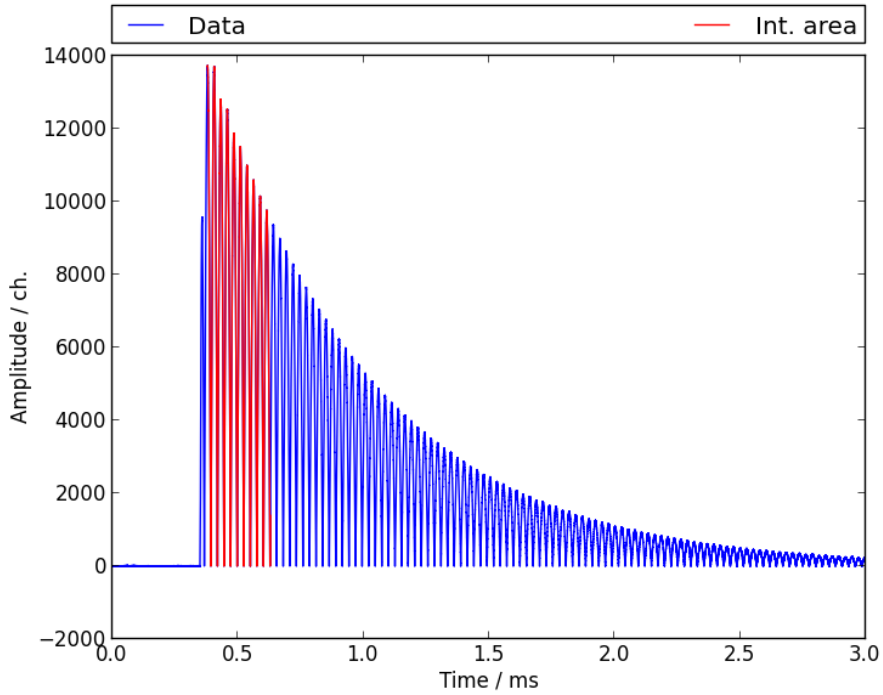

Figure 6: Absolute value or RT signal. Charge calculation may be based on the signal area, instead of the signal amplitude.